Winter 2-16-2005

Quantitative 1H magnetic resonance spectroscopic imaging determines therapeutic immunization efficacy in an animal model of Parkinson's disease.

Michael D. Boska
University of Nebraska Medical Center, mboska@unmc.edu

Travis B. Lewis
University of Nebraska Medical Center

Christopher J. Destache
University of Nebraska Medical Center

Eric J. Benner
University of Nebraska Medical Center

Jay A. Nelson
University of Nebraska Medical Center

See next page for additional authors

Neurobiology of Disease

Quantitative ^{1}H Magnetic Resonance Spectroscopic Imaging Determines Therapeutic Immunization Efficacy in an Animal Model of Parkinson's Disease

Michael D. Boska,[1,2] Travis B. Lewis,[1] Christopher J. Destache,[1,4] Eric J. Benner,[1] Jay A. Nelson,[1,2] Mariano Uberti,[1,2] R. Lee Mosley,[1,3]* and Howard E. Gendelman[1,3]*

[1]Center for Neurovirology and Neurodegenerative Disorders, Departments of [2]Radiology and [3]Pharmacology, University of Nebraska Medical Center, Omaha, Nebraska 68198-5215, and [4]Department of Pharmacy Practice, College of Pharmacy, Creighton University Medical Center, Omaha, Nebraska 68131

Nigrostriatal degeneration, the pathological hallmark of Parkinson's disease (PD), is mirrored by 1-methyl-4-phenyl-1,2,3,6-tetrahydropyridine (MPTP) intoxication. MPTP-treated animals show the common behavioral, motor, and pathological features of human disease. We demonstrated previously that adoptive transfer of Copaxone (Cop-1) immune cells protected the nigrostriatal dopaminergic pathway in MPTP-intoxicated mice. Herein, we evaluated this protection by quantitative proton magnetic resonance spectroscopic imaging (^{1}H MRSI). ^{1}H MRSI performed in MPTP-treated mice demonstrated that *N*-acetyl aspartate (NAA) was significantly diminished in the substantia nigra pars compacta (SNpc) and striatum, regions most affected in human disease. When the same regions were coregistered with immunohistochemical stains for tyrosine hydroxylase, numbers of neuronal bodies and termini were similarly diminished. MPTP-intoxicated animals that received Cop-1 immune cells showed NAA levels, in the SNpc and striatum, nearly equivalent to PBS-treated animals. Moreover, adoptive transfer of immune cells from ovalbumin-immunized to MPTP-treated mice failed to alter NAA levels or protect dopaminergic neurons and their projections. These results demonstrate that ^{1}H MRSI can evaluate dopaminergic degeneration and its protection by Cop-1 immunization strategies. Most importantly, the results provide a monitoring system to assess therapeutic outcomes for PD.

Key words: Parkinson's disease; murine model; ^{1}H MRSI; spectroscopic quantitation; immune therapy; copolymer-1

Introduction

Parkinson's disease (PD) is a common and debilitating neurodegenerative disorder. Symptoms of tremor, rigidity, bradykinesia, and postural instability commonly progress to significant movement and cognitive dysfunction. Pathological changes in the substantia nigra pars compacta (SNpc) and striatum consist of nigral dopaminergic neuronal loss, intraneuronal cytoplasmic inclusions or "Lewy Bodies," gliosis, and striatal dopamine depletion (Lang and Lozano, 1998; Braak and Braak, 2000; Fahn and Przedborski, 2000). Innate immunity involving resident microglial cells with secretion of neurotoxic cytokines and production of reactive oxygen and nitrogen species can contribute to nigrostriatal dopaminergic degeneration (Gao et al., 2003).

Behavioral and neuropathological outcomes of human disease are mirrored in 1-methyl-4-phenyl-1,2,3,6-tetrahydropyridine (MPTP)-intoxicated animals (Wu et al., 2003). Such animals demonstrate degeneration of the nigrostriatal system characterized by diminished dopamine, neuronal and termini loss (Tanji et al., 1999; Bezard et al., 2001), and glial inflammation (Gao et al., 2003). For the latter, attenuating brain inflammation can affect the disease process (He et al., 2001). In a recent report from our laboratories, immune cells recovered from Copaxone (Cop-1; glatiramer acetate)-vaccinated animals and injected into MPTP-treated animals entering inflamed brain regions, increased expression of astrocyte glial cell line-derived neurotrophic factor (GDNF), and attenuated microglial responses. These effects parallel protection of the nigrostriatal pathways (Benner et al., 2004). Importantly, both microglial deactivation and GDNF administration into the caudate and putamen show potential clinical benefit (Gill et al., 2003; Kirik et al., 2004). Cop-1 immunization generates nonencephalitic T cells that cross react with myelin basic protein, elicits few side effects (Johnson, 1996; Teitelbaum et al., 1997; Aharoni et al., 1999; Chen et al., 2001), and shows efficacy for relapsing-remitting multiple sclerosis (Johnson, 1996; Chen et al., 2001). The ability of Cop-1 to affect immune system responses in animal models of neurodegenerative disorders supports its potential for human use (Angelov et al., 2003; Benner et al., 2004; Kipnis et al., 2004b).

Clinical responses may be limited by the timing of therapeutic intervention. Currently, PD is commonly diagnosed when >50% of SNpc neurons and their terminals are destroyed (Bernheimer

Received Oct. 20, 2004; revised Dec. 23, 2004; accepted Dec. 23, 2004.

This work was supported in part by the Alan and Marcia Baer Foundation, the Francis Veitzer Blumkin Foundation, and National Institutes of Health Grants 2 R37 NS36126, 1T32, NS07488 (H.E.G.), 1R21 NS049264 (R.L.M.), 1P01 NS043985-01, 5P01 MH64570-03, and P20 RR15635 (H.E.G., M.D.B.). We thank Dr. Hoby Hetherington for useful discussions and aid in software development and Robin Taylor for excellent editorial assistance.

*R.L.M. and H.E.G. contributed equally to this work.

Correspondence should be addressed to Dr. Michael D. Boska, Department of Radiology, 981045 University of Nebraska Medical Center, Omaha, NE 68198-1045. E-mail: mboska@unmc.edu.

DOI:10.1523/JNEUROSCI.4364-04.2005

 0270-6474/05/251691-10$15.00/0

et al., 1973). An early diagnosis would enable early treatment intervention at times when positive outcomes are likely. In this regard, functional imaging, including single-photon emission computerized tomography (SPECT) (Seibyl et al., 1995; Benamer et al., 2000), positron emission tomography (PET) (Vingerhoets et al., 1994; Eidelberg et al., 1995a,b; Morrish et al., 1996), proton magnetic resonance spectroscopic imaging (^{1}H MRSI) (Cruz et al., 1997; Tedeschi et al., 1997), and functional magnetic resonance imaging (MRI) (Ceballos-Baumann, 2003), are promising approaches for early PD diagnosis. The potential for detection of early disease stage is significant (Burn and O'Brien, 2003; Simpkins and Jankovic, 2003).

With this in mind, we developed high-spatial resolution ^{1}H MRSI to monitor PD-affected brain subregions, the SNpc and striatum. Analysis demonstrated that *N*-acetyl aspartate (NAA) was reduced in the SNpc of MPTP mice. Significantly higher [NAA] was seen in MPTP mice that received Cop-1 immune cell-adoptive transfers than in MPTP or MPTP/ovalbumin (OVA) animals. We demonstrate that [NAA] can assess nigrostriatal degeneration and therapeutic responses for MPTP intoxication.

Materials and Methods

Animals. Male SJL/J mice were purchased from The Jackson Laboratory (Bar Harbor, ME) and placed in study at 6–10 weeks of age. All animal procedures were in accordance with National Institutes of Health guidelines and were approved by the Institutional Animal Care and Use Committee of the University of Nebraska Medical Center.

Immunization, MPTP intoxication, and adoptive cell transfers. Donor mice were immunized with 200 μg of either Cop-1 or OVA emulsified in 0.2 ml of complete Freund's adjuvant (CFA) containing 1 mg/ml mycobacterium tuberculosis (Sigma, St. Louis, MO) injected subcutaneously at two lateral sites at the tail base. Recipient mice received four intraperitoneal injections at 2 h intervals of either vehicle (PBS, 10 ml/kg) or MPTP-HCl (18 mg/kg free base; Sigma) in PBS. MPTP safety measures were in accordance with guidelines published previously (Przedborski et al., 2001). Five days after immunization, donor mice were killed, and single-cell suspensions were prepared from pooled draining inguinal lymph nodes and spleens. Twelve hours after the last MPTP injection, random mice received intravenously 5–10 $\times$ 10^7 immune cells from Cop-1- or OVA-immunized donor mice or no splenocytes (n = 5–9 mice per group) in 0.25 ml of HBSS. On days 2 and 6 after MPTP intoxication, brain metabolites were evaluated by ^{1}H MRSI.

MRI/MRSI. MRI and MRSI were obtained using a Bruker (Ettlingen, Germany) Avance 7T/21 cm system, operating at 300.41 MHz, using actively decoupled 72 mm volume coil transmit and a laboratory built 1.25 $\times$ 1.5 cm receive surface coil. MR images were acquired with a 20 mm field of view (FOV), 25 contiguous 0.5 mm thick slices with interleaved slice order, 128 $\times$ 128 matrix, and eight echoes with 15 ms echo spacing and were refocused with Carr-Purcell-Meiboom-Gill (CPMG) phase-cycled radiofrequency refocusing pulses to form eight images used for T_2 mapping and coregistration with histology. Spectroscopic images were obtained using a numerically optimized binomial excitation (Hetherington, 1994) refocused using three orthogonal slice-selective refocusing pulses [binomial excitation with volume-selective refocusing (BEVR)] (Boska et al., 2003). Spectroscopic images were obtained by selecting an 8 $\times$ 4.2 $\times$ 1.5 mm volume of interest, using 24 $\times$ 24 spatial encoding over a 20 mm FOV in the slice containing the SNpc yielding a nominal voxel size of 1 μl, 16 $\times$ 16 encoding over the slice containing the striatum (2.33 μl of voxel), and echo time (TE) of 33 ms, repetition time (TR) of 4 s, and receiver gain of 50,000, two averages. The total acquisition time was 80 min for the SNpc and 40 min for the striatum. Shimming of the selected volume used Fastmap (Gruetter, 1993) for initial shims, with the final shim on the selected volume performed manually to achieve a final water line width of 10–15 Hz.

MRSI processing. Spectroscopic images were Fourier transformed in the phase-encoding dimensions and reformatted using MatLab (MathWorks, Natick, MA). Spectra were fit using advanced method for accurate, robust, efficient spectral fitting (AMARES) (Vanhamme, 1997) in the Java-based magnetic resonance user's interface (jMRUI) package (Naressi, 2001). Model parameters and constraints were generated using spectra from phantoms. Each was done separately for Cre, Cho, NAA, glutamate, glutamine, myoinositol, taurine, lactate, or glucose with 3-(trimethylsilyl)-1-propane-sulfonic acid and sodium formate as chemical shift and phasing references. Phantoms of each metabolite were prepared in pH 7.5 phosphate buffer (100 mM) and maintained at 38°C during spectral acquisition using a circulating water jacket.

Brain metabolites. Unsuppressed water spectroscopic images were obtained with identical metabolite spectra parameters except for the following: TR = 1 s, numerical aperture (NA) = 1, and receiver gain = 1000. The unsuppressed water was used as an internal standard for each voxel to quantitate metabolite concentrations from the water-suppressed MRSI data (Husted et al., 1994). Water spectra were fit in the time domain to a single exponential decay. Water line width was used to measure long T_2 singlet line widths within each voxel to constrain the metabolite fitting routine. Water and metabolite signal amplitudes were corrected for T_1 and T_2. To calculate metabolite concentrations, the major peak in the spectrum of each metabolite was corrected for number of averages and number of protons contributing to the peak. A technologist, blinded to the data source, fit the data. Calibration of the ratio of metabolite to water signal amplitude at the respective receiver gains was measured in phantom studies. Calculations were performed using MatLab (MathWorks), and metabolite concentrations were output as American standard code for information interchange (for database development) and binary (for MRI overlay) metabolite maps.

Water and metabolite T_1 and T_2. Metabolite T_2 data sets (20, 33, 50, 75, 100, 136, 175, 225, and 272 ms TE) were acquired using a PRESS pulse sequence with WET water suppression (Ogg et al., 1994). Single voxel spectra were obtained for T_2 measurements from a 4 $\times$ 3 $\times$ 2 mm voxel placed in the basal ganglia with 3 kHz bandwidth, 4096 points, TR = 4 s, and NA = 128 for a total spectral acquisition time of 8 min 32 s per spectrum at each TE. Metabolite inversion recovery T_1 data sets were acquired using the BEVR pulse sequence from the same voxel as the T_2 data. Single-voxel spectra for metabolite T_1 data sets used 3 kHz bandwidth, 4096 points, TR = 10–20 s, NA = 128, TE = 33 ms, and nine TI values (51, 100, 200, 400, 700, 1000, 2000, 4000, and 10,000 ms), with a 10 s preinversion delay yielding an acquisition time of 8–16 min per spectrum.

Water T_2 was determined using an eight echo CPMG phase-cycled spin-echo MRI sequence with a 12 ms echo spacing. Water T_1 was determined using an eight-TR (400–10,000 ms) progressive saturation imaging experiment. Data were fit on a voxel by voxel basis using programs written in C. Images were acquired in the coronal plane with 20 mm FOV, 0.5 mm slice thickness, 128 $\times$ 128 matrix, interleaved slice acquisition, and 25 contiguous slices.

MRI and histological coregistration. Digital images were preprocessed by subimaging the brain from both the MRI T_2 maps and digitized images of coronal histological sections stained for TH expression. Pixel dimensions in digital images of TH-visualized sections were separately measured on *x*, *y*, and *z* axes based on MRI, and a rigid model for three-dimensional head-in-hat coregistration of histology to MRI was achieved using the AIR registration package (Woods et al., 1998) in the MedX software suite (Sensor Systems, Sterling, VA). MRI was used to measure voxel dimensions of digitized histology independently in *x*, *y*, and *z* to account for tissue shrinkage. Errors in image coregistration were minimized by using the MRI as the source of truth and placing the voxel based on anatomical features identified on the histology slice in cases in which visual disagreement could be identified by mouse brain anatomical experts.

Voxel selection. MRSI voxels (one per hemisphere) containing the SNpc, not visible on the MRI, were selected using neuroanatomical landmarks and validated using coregistered TH-stained histological sections as detailed in MRI and histological coregistration. SNpc voxel placement was shifted in the original time domain data sets to encompass the SNpc as needed. Voxels centered within the striatum (one per hemisphere) were selected based on MRI.

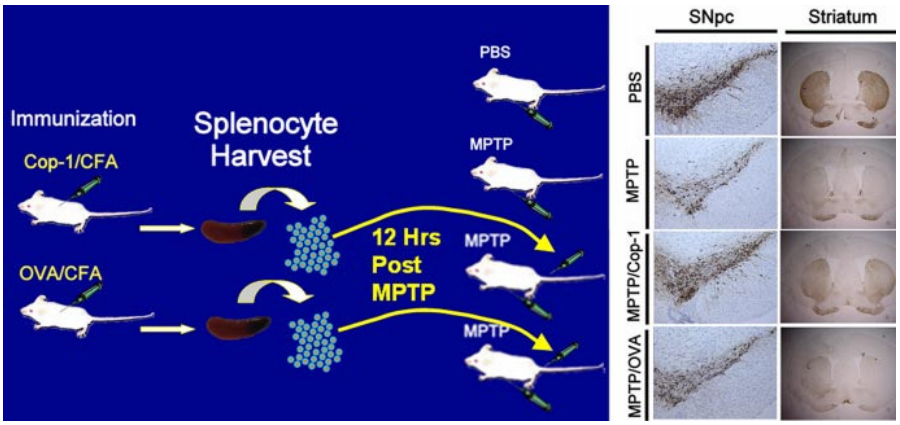

Figure 1. Experimental design demonstrates neuroprotective activities of Cop-1 splenocytes. Shown here is the time course of animal treatment (left panel) and immunohistochemical staining (right panel) for TH in the SNpc and striatum of mice treated with PBS, MPTP, or adoptively transferred splenocytes from donors immunized with either Cop-1 (MPTP/Cop-1) or ovalbumin (MPTP/OVA).

Immunohistochemistry and neuronal quantitation. After day 6, mice tested by MRSI were killed by a pentobarbital overdose and perfused with PBS followed by 4% paraformaldehyde. Brains were harvested, postfixed with 4% paraformaldehyde, cryoprotected in 30% sucrose, and processed for immunohistochemical studies. Processed brains were embedded in OCT medium, and 25 μm coronal sections were cut throughout the brain. Every 10th section was mounted onto slides for coregistration and, every fifth serial section maintained as free-floating tissue was stained for TH. Mounted sections were incubated with a 1:500 dilution of rabbit polyclonal anti-TH (Calbiochem, La Jolla, CA; Novabiochem, San Diego, CA), whereas free-floating tissues were reacted with a 1:2000 antibody dilution. Anti-TH immunoglobulin was detected with a 1:200 to 1:400 dilution of biotinylated goat IgG anti-rabbit Ig, followed by streptavidin-conjugated horseradish peroxidase (HRP) (Vectastain ABC kit; Vector Laboratories, Burlingame, CA). HRP was visualized with 3,3′-diaminobenzine (DAB) after reaction with hydrogen peroxide (DAB kit; Vector Laboratories). All sections were counterstained with thionine for Nissl substance. Immunohistochemical-stained tissues from slides mounted before reactions spanned the three 500 μm MRI sections corresponding to the ^{1}H MRSI slice and were coregistered with MRI for validation of voxel placement (see MRI and histological coregistration). Total numbers of TH- and Nissl-stained neurons in SNpc were determined from free-floating tissues and quantified by stereological tests using the Optical Fractionator probe of Stereo Investigator software (MicroBrightField, Williston, VT) (Liberatore et al., 1999). Laboratory personnel were blinded to the identity of the histological sections being counted.

Reverse-phase HPLC (RP-HPLC). [NAA] in ventral midbrains was analyzed by HPLC at 2 d after MPTP intoxication. Briefly, cohorts of mice congruently treated as described previously were killed by CO_2 asphyxiation. Ventral midbrains were immediately dissected, flash frozen, and stored at −80°C until analyzed. Before analysis, frozen tissues were weighed, resuspended in 10 volumes of 0.1N aqueous perchloric acid, and homogenized with a motorized pestle. Tissues were clarified by centrifugation at 12,000 × *g* for 10 min, and 250 μl of each supernatant was removed for RP-HPLC analysis (Shimadzu, Columbia, MD). [NAA] was evaluated by anion exchange RP-HPLC (Sager et al., 1995) through a C_{18} BetaBasic column (4.6 × 100 mm) and a BioBasic strong cation exchange column (4.6 × 150 mm) connected in tandem (Thermo-Electron, Walthman, MA). Analytes were eluted with 25 mM KCl HPLC-grade water containing 5N NaOH and 10N H_2SO_4, pH 4.5, and detected at a wavelength of 210 nm by UV-Vis detection (SPD-10Avp; Shimadzu). Freshly prepared NAA standards were assessed for each determination. Daily variation between each determination for 10 μg/ml of NAA was 5.8%, and the correlation coefficients for all standard curves were ≥0.992.

Statistical tests. Analyses were undertaken to examine treatment differences in [NAA], [Cre], and [Cho] within selected regions of interest for both SN and striatum. Analyses also examined the differences in TH$^+$- and Nissl-stained neuronal counts within each voxel containing the SNpc and the entire lesion for each mouse. Neuronal counts found outside of the 99% confidence interval within each group were eliminated from the data set. Linear and logistic regression models were applied to the data along with generalized estimating equations to account for within subject correlation. Models originally included effects for right/left hemisphere and time in addition to treatment effect, but because no differences in hemisphere or time were discerned, these were removed from the model. If differences were found, pair-wise comparisons between all treatment groups were determined by the Bonferroni procedure. Comparisons of individual time points were performed using a Dunnett T3 test for comparisons of values between each time point and group without assumption of normal value distribution. All analyses were performed using SPSS for Windows (version 12; SPSS, Chicago, IL).

Results

^{1}H MRSI tests were used as a noninvasive measure of the nigrostriatal dopaminergic system in MPTP-intoxicated animals. Quantitative ^{1}H MRSI profiles were obtained from coronal slices of the SNpc and striatum in MPTP-treated animals that received Cop-1 or OVA splenocytes (MPTP/Cop-1 and MPTP/OVA). The SNpc and striatum were examined by immunohistological tests coregistered from brain subregions where spectra were acquired. The results support our previous work showing that adoptive transfer of Cop-1 splenocytes to MPTP-treated mice led to significant protection of the dopamine striatal system (Benner et al., 2004). Figure 1 demonstrates the treatment protocol and typical TH$^+$ neuronal stains in SNpc and striatum for each treatment group. In these studies, donor mice were immunized with CFA containing either Cop-1 or OVA (Fig. 1, left), and splenocytes were harvested after 5 d and adoptively transferred to recipient mice 12 h after MPTP intoxication. As reported previously (Benner et al., 2004), MPTP induced a significant loss of TH-immunoreactive neuronal bodies in the SNpc and termini in the striatum (Fig. 1, right). Adoptive transfer of splenocytes from Cop-1 immunized mice (MPTP/Cop-1-treated group) attenuated the MPTP-induced TH$^+$ neuronal (SNpc) and striatal termini loss, whereas adoptive transfer of OVA cells had no such effects (MPTP/OVA). We next investigated ^{1}H MRSI as a noninvasive measure of immune-based therapy in MPTP-treated mice. ^{1}H MRSI monitoring of neurological damage by [NAA] reflects neuronal damage in a variety of animal models of neurodegenerative disease (Podell et al., 1999; Kitada et al., 2000; Matalon et al., 2000; Chung et al., 2003; Vielhaber et al., 2003). Nonetheless, significant challenges were encountered obtaining spectroscopic images in mouse brain as a result of the requirement for high-spatial resolution. Thus, we first developed protocols for a high-field (7 tesla) MR system.

Results of data acquisition, analysis, display, and database development are shown in Figure 2. The developed pulse sequence was specifically designed to eliminate problems of residual water, lipids, and stimulated echoes, which effect high-field ^{1}H MRSI spectral integrity. In this regard, an extension of a method used for high-field (4.1 tesla) human ^{1}H MRSI (Hetherington, 1994) was established using numerically optimized BEVR (Boska et al., 2003) (Fig. 2*A*). This optimization provided robust spectro-

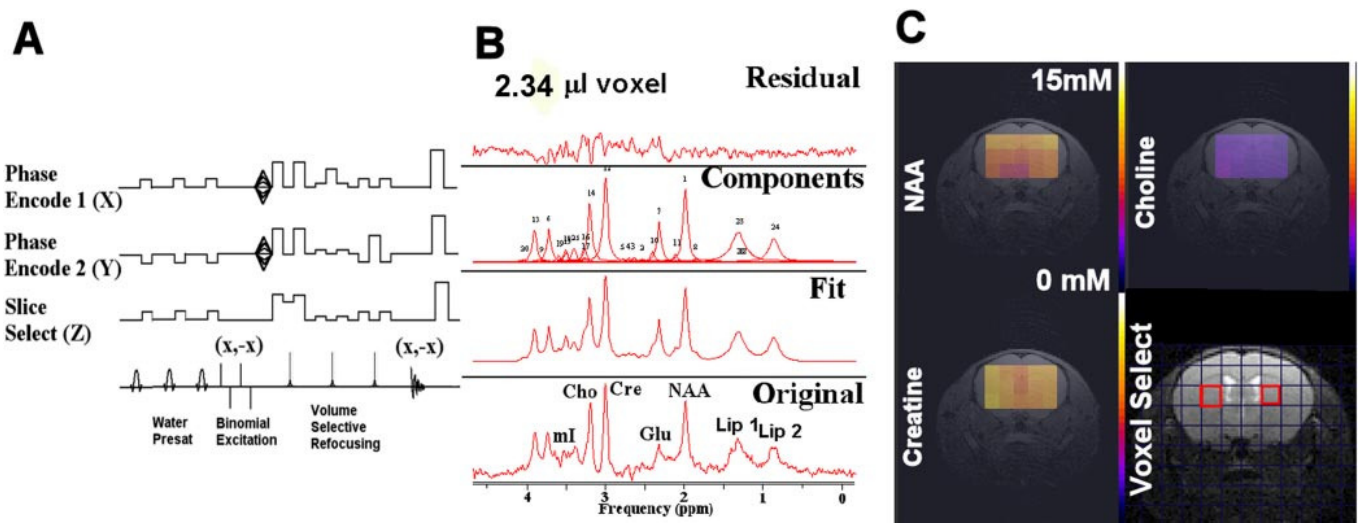

Figure 2. ^{1}H MRSI data acquisition and processing. *A*, The data acquisition used a BEVR sequence preceded by water presaturation and gradient spoiling. *B*, Spectra from all voxels were fit in the time domain using AMARES in the jMRUI package. The example shown is a representative fit from a single voxel within the ^{1}H MRSI data set of the striatum. *C*, Output from the AMARES fits was compiled into metabolite maps used to generate quantitative overlays, as shown here, and a database of metabolic concentrations. Metabolite concentrations within the voxels of the striatum or SNpc were extracted from the database and statistically analyzed.

Table 1. T_1 and T_2 determinations of metabolites and tissue water

Basal ganglia metabolite relaxation times[a]		
Metabolite	T_1 (ms) ($n = 5$)	T_2 (ms) ($n = 8$)
N-acetylaspartate	1380 ± 100	154 ± 16
Creatine	1360 ± 130	105 ± 7
Choline	1270 ± 130	139 ± 33
Taurine	1390 ± 510	127 ± 98
Glutamate	1250 ± 210	33 ± 5
Glutamine	1200 ± 220	24 ± 19
Myoinositol	1020 ± 140	28 ± 8
Tissue water (SNpc)	1866 ± 219	44.0 ± 2.2
Tissue water (striatum)	2066 ± 139	46.2 ± 2.7

[a]Mean ± SD for five to eight mice per determination.

scopic imaging. Figure 2*B* illustrates a curve fit used to measure multiple brain metabolites. Results from curve fit and quantitation were reformatted into metabolite maps for image overlays (Fig. 2*C*). Voxels corresponding to the regions of interest encompassing the SNpc and within the striatum were identified (Fig. 2*C*, bottom right) and entered into the database. Quantitation was performed by referencing the water signal in an unsuppressed voxel. To correct amplitudes for magnetic saturation, T_1 and T_2 values of both metabolites and tissue water were measured. Typical values for water and tissue T_1s and T_2s are displayed in Table 1.

To identify the MRSI voxel containing the SNpc, TH-immunostained coronal sections were coregistered with MRI. An example of TH-immunostained histological sections coregistered to T_2 maps is displayed in Figure 3. Placement of the voxel of interest was validated by immunocytochemistry to represent TH^+ neuronal SNpc cell bodies. Examples of the voxels (one/hemisphere) selected from a single animal in both the SNpc and striatum are displayed in Figure 4. Details of the three contiguous 0.5 mm MRI slices and corresponding coregistered histology for each 1.5 mm ^{1}H MRSI slice are shown in Figure 4, *A* and *B*. Coregistration and voxel identification were used for counting TH^+- and Nissl-stained neurons by stereology. These methods, while not allowing a pixel-by-pixel correlation between the two data sets, allowed regional matching for correlating spectroscopic tracings with immunostaining results through selected volume measurement.

The primary metabolic effect of MPTP treatment was the reduction of [NAA] in the region of the SNpc. Figure 5 shows MRSI analyses of coronal brain slices and example spectra from single voxels containing the SNpc (arrows) of mice from each treatment group evaluated at day 2 after MPTP. A reduction of NAA levels in SNpc of MPTP and MPTP/OVA-treated mice is shown. Similar trends in Cre and Cho concentrations from the same mice were, on average, not observed. However, detectable changes in individual spectra (data not shown) were found. For example, in the individual spectrum shown for the COP-1-treated animal, a reduction of creatine is apparent, which was not found statistically. This highlights the need for comprehensive comparison of individual results from animals with histopathology, biochemical assays, and proteomics results to evaluate not just treatment effects but also details of individual biological response. Evaluation of the entire cohort revealed that [NAA] was significantly reduced in the SNpc of MPTP ($p = 0.02$) and MPTP/OVA ($p = 0.05$) treatment groups (Fig. 6). [NAA] remained at control concentrations following adoptive transfer of Cop-1 splenocytes (MPTP/Cop-1) ($p = 0.90$ vs PBS). [NAA] in the striatum was not changed in any treatment group ($p = 0.73$). However, trends of diminished [NAA] in MPTP animals were reversed in animals that received Cop-1 splenocytes (MPTP/Cop-1) but not in those that received OVA splenocytes (MPTP/OVA). The concentration of [Cre] and [Cho] in SNpc and striatum on days 2 and 6 are shown in Table 2. No statistical differences in [Cho] among any treatment group at either time point or afflicted brain region were seen. Dunnett T3 yielded a significantly lower [Cre] within the striatum of MPTP mice at day 2 ($p = 0.03$) that had recovered by day 6 ($p = 0.93$) compared with PBS-treated mice. The mechanism for this transient effect is unclear. Notably, [NAA] of PBS-treated controls was significantly lower in the striatum (7.4 ± 0.2 mM) than in the SNpc (9.6 ± 0.4 mM) ($p < 0.001$). In addition, PBS mice showed significantly greater [Cho] in the striatum (2.7 ± 0.1 mM) than in the SNpc (2.2 ± 0.2 mM; $p = 0.01$). However, differences in [Cre] in the SNpc and striatum of PBS-treated mice were not found ($p = 0.37$).

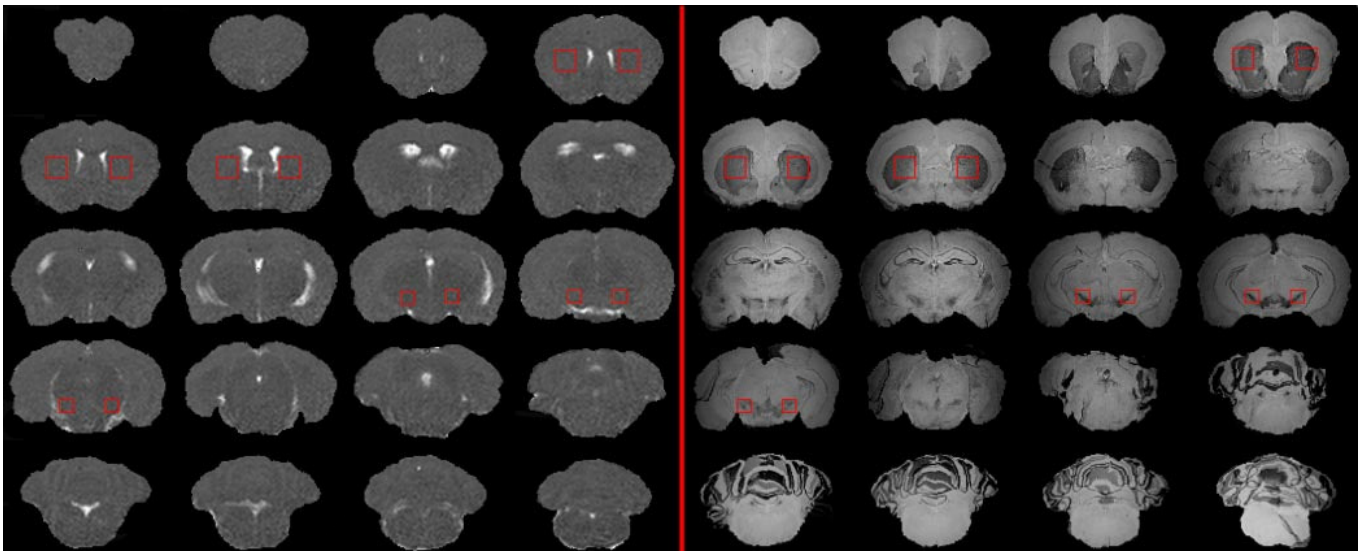

Figure 3. Three-dimensional head-in-hat coregistration of histological sections photographed at 500 μm intervals (right) with contiguous 500 μm slices. T_2 maps were subimaged from 8-echo CPMG phase-cycled MRI (left). Slices corresponding to the position of the striatum and SNpc were used to identify voxel locations (red boxes) for spectral analysis. Corresponding boxes on the histological data were used as a guide to stereological analysis for Nissl-stained and TH-immunoreactive neuronal counts within the voxel and spectroscopic data.

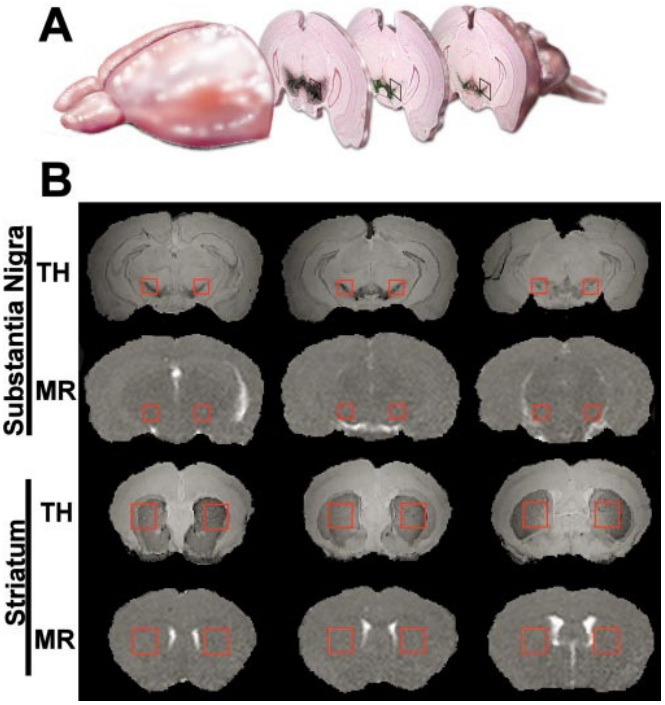

Figure 4. Voxel selection in the SNpc and striatum. *A*, Three-dimensional cartoon of the voxel of interest selected for SNpc spectral measurement and stereological tests. *B*, TH antigen expression (top row) coregistered to subimaged T_2 map (second row) in the SNpc. TH expression in the striatum (third row) coregistered to subimaged T_2 map (bottom row). Red boxes demonstrate the selection of the volumes identified as SNpc (top 2 rows) or striatum (bottom 2 rows).

To determine the degree of neuronal loss corresponding to the observed metabolic changes, Immunohistological-stained sections were analyzed by stereological tests of matched MRI regions (those contained in the voxel of interest) encompassing the SNpc. Both TH^+- and Nissl-stained neurons within the voxel analyzed for metabolite concentrations were counted in each animal after the second ^{1}H MRSI examination (day 6). This was done to compare neuronal loss with metabolic changes. Neuronal counts are shown in Table 3. MPTP treatment caused a loss of 22% of the dopaminergic neurons ($p = 0.014$ vs PBS) within the selected volume, and MPTP/OVA splenocyte treatment showed a 33% loss ($p = 0.016$ vs PBS). Neuronal counts within voxels from mice that received Cop-1 splenocytes were partially spared (11% loss) compared with those from MPTP intoxication (22%) and were not different from TH^+ neuronal counts from PBS controls ($p = 0.456$ vs PBS). No statistically significant differences in Nissl-stained (TH-negative) neurons were observed in any group when compared with PBS controls. Comparison of [NAA] and TH^+ neuronal counts demonstrated a weak correlation ($r = 0.582$; $p = 0.001$; Pearson correlation) between neuronal counts and [NAA] in MPTP and MPTP/OVA-treated mice and in MPTP/Cop-1-treated mice (Fig. 7).

[NAA] in the SNpc and striatum, measured by quantitative ^{1}H MRSI, was compared with [NAA] detected by HPLC at day 2 in all animal groups (Table 4). Tissue in the ventral midbrain of the basal ganglia, which includes the SN, was used. Concomitant reductions of [NAA] in the SNpc as measured by ^{1}H MRSI were also reflected by HPLC analysis of the ventral midbrain. Although trends toward [NAA] changes as an effect of treatment were similar for ^{1}H MRSI and HPLC, absolute quantitative agreement between the two methods was not achieved (Table 4).

Together, these results demonstrate that measurements of absolute [NAA] by ^{1}H MRSI analysis within and around the SNpc is suitable for monitoring MPTP induced degeneration of the nigrostriatal pathway as well as immune-based neuroprotective therapy in this model of PD. In addition, other metabolic changes were detected, including transient reductions in [Cre] on day 2 in the striatum resulting from MPTP intoxication, which was reversed by Cop-1 immune cells.

Discussion

PD is characterized by slow and progressive degeneration of the nigrostriatal dopaminergic pathway (Lang and Lozano, 1998; Langston et al., 1999; Dawson and Dawson, 2003). Currently, approved treatment modalities for PD remain only palliative (Shults, 2003). We previously demonstrated that attenuation of microglial responses and adoptive transfer of Cop-1-specific immune cells into MPTP-treated animals can achieve glial expres-

sion of GDNF. Such responses parallel the protection of dopaminergic neurons and their striatal projections in Cop-1/MPTP mice (Benner et al., 2004).

No laboratory tests for PD currently exist. Thus, history and neurological examination remain the principal diagnostic methods. Disease manifests only after significant damage, typically >50% neuronal loss, occurs to the SNpc (Bernheimer et al., 1973). Most commonly, symptoms begin insidiously and consist of bradykinesia and resting tremor and progress to immobility and balance difficulties. Disease manifestations in patients over the age of 65 are misdiagnosed as arthritis, depression, and global weakness (Wolters, 2000, 2001; Garber and Friedman, 2003). Behavioral and mental disorders, including dementia, can occur together with motor dysfunction, but cognitive deficits usually occur only late in the course of disease (Locascio et al., 2003). Levels of fluoro-L-3,4-dihydroxyphenylalanine (L-DOPA) and dopamine transporters are used to assess L-DOPA uptake and dopaminergic nerve terminals through PET or SPECT analyses, respectively (Vingerhoets et al., 1994; Eidelberg et al., 1995a,b; Seibyl et al., 1995; Morrish et al., 1996; Benamer et al., 2000); however, both require substantial neural damage to register significant discrimination from normal and attain diagnostic sensitivity. Thus, together, a definitive diagnosis of PD requires substantive clinical manifestations (DeKosky and Marek, 2003).

In our current study, we used high-field ^{1}H MRSI with histological coregistration to measure, in a sensitive and specific manner, nigrostriatal dopaminergic degeneration. Such measurements allowed quantitative analysis of neuroprotective events that follow adoptive transfer of Cop-1 immune cells. Previous studies using single-voxel ^{1}H MRSI showed reduced NAA/Cho ratios in the SN and thalamus of PD patients that were reversed after successful stereotactic thalamotomy, a procedure used to control symptoms in medically intractable PD (Baik et al., 2003). MRSI analysis of the striatum has yielded inconsistent results. One study demonstrated increased [Cho] in the striatum for which the biological significance is not clear (Clarke and Lowry, 2001) but may be reflective of inflammatory responses in PD patients. ^{1}H MRS in MPTP-intoxicated cats demonstrated reduced striatal [NAA] (Podell et al., 2003); however, the degree of feline MPTP intoxication was pathologically more severe than induced in our study. Our data demonstrate that ^{1}H MRSI and specifically [NAA] reflect dopaminergic loss in MPTP-intoxicated mice and can be used to monitor putative neuroprotective therapies.

Previous work from our laboratory and from others demonstrate that adaptive immune responses provide neuroprotection against secondary damage after a variety of neural insults, including MPTP intoxication (Benner et al., 2004), traumatic injury of motor neurons and optic nerve (Moalem et al., 1999; Kipnis et al., 2000; Angelov et al., 2003), the superoxide dismutase 1 mutation causing amyotrophic lateral sclerosis (ALS) (Angelov et al., 2003), retinal ganglion toxicity by glutamate (Schori et al., 2001), and neurotransmitter imbalance by dizocilpine maleate and amphetamines (Kipnis et al., 2004). Cop-1 induces autoimmune T-cells preventing additional degeneration of the CNS after ini-

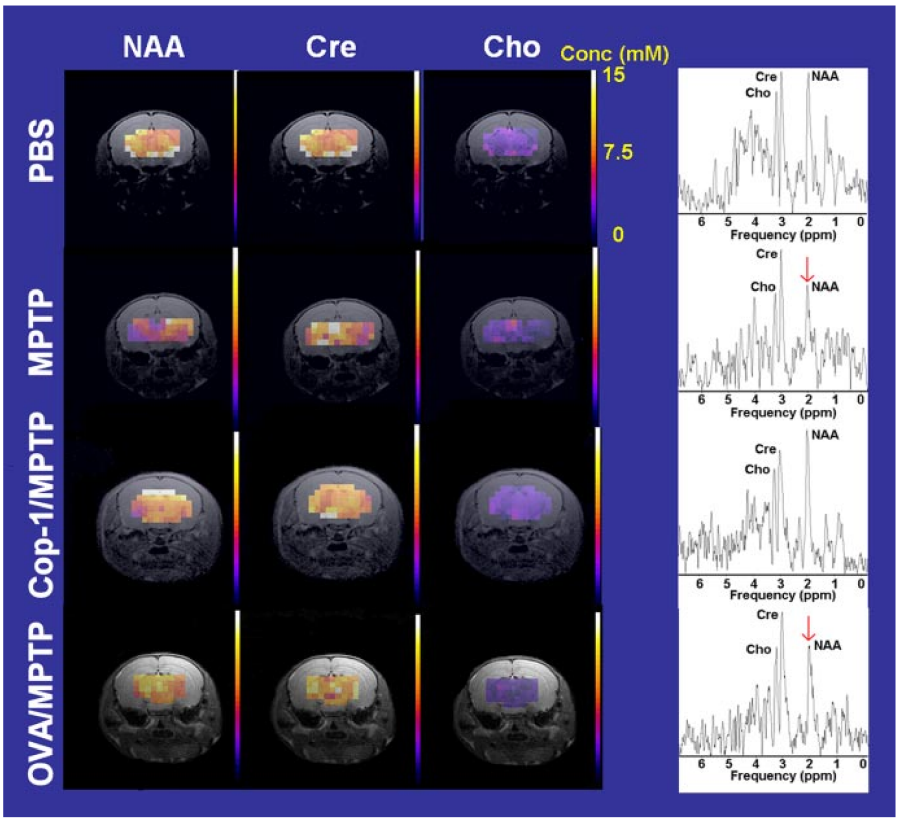

Figure 5. [NAA], [Cre], and [Cho] overlays in SN containing brain slices with representative single-voxel spectra from voxels containing SNpc. Concentration maps of NAA (left), Cre (center, left), and Cho (center, right) for representative mice treated with PBS (top row), MPTP (second row from top), MPTP/Cop-1 (third row from top), or MPTP/OVA immune donors (bottom row). The vertical color bar is a color code for metabolite concentrations ranging from 0 mM (black) to 15 mM (white) on a linear scale (top right). Lower [NAA] in the SNpc (arrows) of MPTP- and MPTP/OVA-treated compared with PBS and MPTP/Cop-1 mice is shown. An extended area of reduced [NAA] surrounds the SNpc in MPTP mice. Representative single-voxel spectra from one voxel containing the SNpc in each of the treatment groups are shown on the right. Significant loss of NAA is apparent in the MPTP and MPTP/OVA treatment groups, whereas NAA is preserved in the MPTP/COP-1-compared with PBS-treated mice.

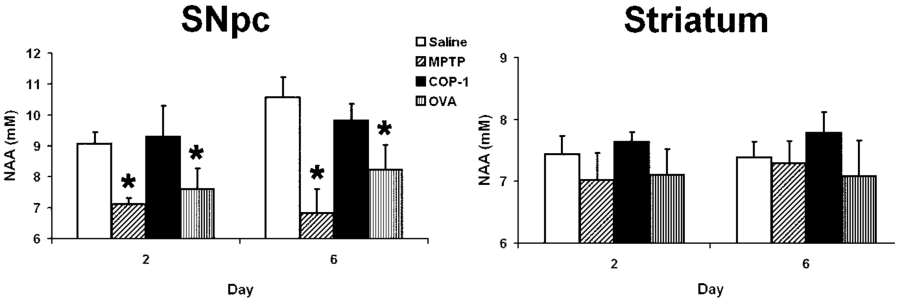

Figure 6. ^{1}H MRSI NAA levels on days 2 and 6 after MPTP treatment. Concentrations of NAA in and around the SNpc (left panel) or striatum (right panel) were measured in mice treated with PBS (white bars), MPTP (side hatched bars), MPTP/Cop-1 (black bars), or MPTP/OVA (vertical hatch bars). Data are means ± SEM of five to nine mice per group. *$p \leq 0.05$ compared with PBS-treated control.

Table 2. ^{1}H-MRSI Cre and Cho levels in the SNpc and striatum in MPTP-treated mice

			Basal ganglia metabolites (mM)[a]			
			Cre		Cho	
Treatment	Day	*n*	SNpc	Striatum	SNpc	Striatum
PBS	2	16	10.5 ± 0.9	10.0 ± 0.3	2.2 ± 0.2	2.7 ± 0.1
	6	10	10.7 ± 0.9	9.8 ± 0.6	2.3 ± 0.3	2.8 ± 0.1
MPTP	2	4	11.6 ± 0.5	8.4 ± 0.7*	1.9 ± 0.2	2.6 ± 0.2
	6	8	11.5 ± 0.6	9.5 ± 0.9	2.7 ± 0.2	2.9 ± 0.2
MPTP/Cop-1	2	10	10.0 ± 0.6	10.6 ± 0.7	2.3 ± 0.2	2.7 ± 0.2
	6	10	12.2 ± 1.2	10.4 ± 1.3	2.7 ± 0.3	3.2 ± 0.3
MPTP/OVA	2	6	10.6 ± 0.8	8.9 ± 0.7	1.6 ± 0.3	2.6 ± 0.2
	6	5	11.7 ± 1.1	9.6 ± 1.0	1.9 ± 0.1	2.7 ± 0.1

[a]Mean ± SEM for five to nine mice per group.

*$p = 0.03$ compared with PBS-treated mice, day 2.

Table 3. Stereological determination of TH$^+$ dopaminergic (SNpc) and Nissl neurons coregistered by MRSI in each hemisphere at 6 d after MPTP treatment

	Midbrain neuron counts per hemisphere[a]			
	Entire SNpc		MRSI voxel	
Treatment	TH[b]	Nissl[c]	TH[b]	Nissl[c]
PBS	4881 ± 84	1598 ± 109	3025 ± 234	7517 ± 832
MPTP	2456 ± 200*	1537 ± 210	2381 ± 189*	7662 ± 385
MPTP/Cop-1	3733 ± 221*	2204 ± 151*	2887 ± 263	8496 ± 347
MPTP/OVA	2991 ± 181*	1813 ± 244	1758 ± 237*	7027 ± 405

[a]Mean ± SEM for five to nine mice per group.

[b]TH immunoreactive.

[c]Nissl stained, TH negative.

*$p \leq 0.05$ compared with PBS-treated mice.

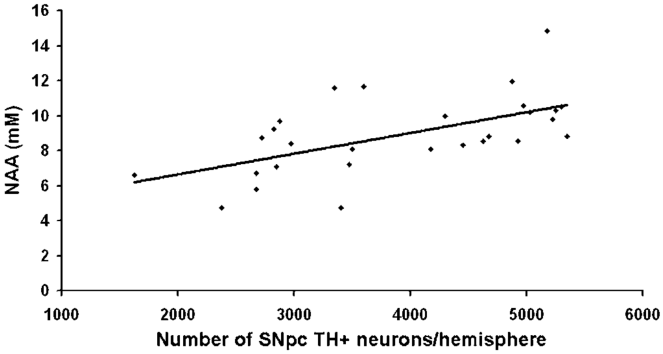

Figure 7. Correlation between the SNpc TH-immunoreactive neurons and ^{1}H MRSI [NAA] levels from mice in all treatment groups. For each mouse, mean [NAA], averaged from both hemispheres, was plotted as a paired function of the number of TH$^+$ neurons per hemisphere, and linear correlation was determined. A modest correlation ($r = 0.582$; $p = 0.001$; Pearson correlation) was found between the loss of dopaminergic neurons and diminution of [NAA].

tial damage. The mechanisms of Cop-1 neuroprotection, including an analysis of the T-cell subtypes involved in the neuroregulatory responses, remain under investigation (Kipnis and Schwartz, 2002).

More specifically, we previously showed protection against MPP$^+$ degeneration of dopaminergic neurons. In that study, the sparing of neuronal and their terminal connections to the striatum was accompanied by increased levels of astrocyte-generated GDNF and interleukin-10 (Benner et al., 2004). It is, nonetheless, likely that COP-1-induced regulatory T-cells affect a number of neuroimmune activities. The balance between proinflammatory and anti-inflammatory cytokines, together with induction of neurotrophins and other growth factors, is likely operative. Direct correlation of *in vivo* changes obtained using quantitative ^{1}H MRSI and quantitative assessment of tissue immunomodulatory factors may, in subsequent works, reveal detailed mechanisms for these neuroprotective processes.

Table 4. NAA concentrations measured by ^{1}H-MRSI and RP-HPLC from the midbrains of mice 2 d after MPTP treatment

	Midbrain NAA levels[A]	
Treatment	MRSI (mM)	HPLC (μmol/g tissue)
PBS	9.1 ± 0.4	16.5 ± 1.5
MPTP	7.1 ± 0.2*	11.0 ± 1.4
MPTP/Cop-1	9.3 ± 1.0	17.5 ± 2.3
MPTP/OVA	7.6 ± 0.7*	13.7 ± 1.4

[a]Mean ± SEM for five to nine mice per group.

*$p \leq 0.05$ compared with PBS-treated mice.

Quantitative MRS is a technique that can be prone to error. The primary source of error is the relaxation (T_1 and T_2) corrections of the signal amplitudes, because these parameters are difficult to measure and can change in pathological conditions. The degree to which this will contribute to potential error increases with decreased repetition time and increased echo time. In addition to difficulties with relaxation properties, difficulties can exist in accurately measuring metabolites near the water resonance because of incomplete water suppression or residual stimulated echoes. For these reasons, we selected acquisition parameters that minimize T_1 and T_2 relaxation corrections (TE, 33 ms; TR, 4 s) and only reported results from metabolites that have long T_2 and are well removed from the spectral regions of residual water and occasional stimulated echoes (NAA, Cre, Cho). Developments have been implemented during the acquisition of these data (Smallcombe et al., 1995) to eliminate residual stimulated echoes to allow for reliable quantitation of a broader array of metabolites in future studies.

As a metabolite found primarily within neurons, measures of NAA are used often as a noninvasive surrogate marker of neuronal integrity for a wide range of neurodegenerative disorders, including stroke, multiple sclerosis, ALS, AD, and human immunodeficiency virus 1-associated dementia (Swindells et al., 1995; Chen et al., 2000; Suhy et al., 2002; Tedeschi et al., 2002; Chung et al., 2003; Schuff et al., 2003). Its use as a diagnostic test for PD has been hampered by the inability of previous tests to precisely localize it to the SNpc, a necessary prerequisite because of the exacting relationship of NAA to neuronal injury and the requirement for high-field MRSI to ensure precise quantitative measurements (Clarke et al., 1997; Cruz et al., 1997; Federico et al., 1997; Brooks, 2000; Clarke and Lowry, 2000; Firbank et al., 2002; Baik et al., 2003). Nevertheless, a number of advantages to NAA measurements are evident, including its exclusive relationship to synthesis in neuronal mitochondria and reduction in mitochondrial dysfunction (Clark, 1998; Signoretti et al., 2001). Such subcellular injury may also be responsible for [NAA] reductions that we observed in and around the SNpc of MPTP-intoxicated animals, which may reflect partial volume effects associated with glutaminergic and GABAergic neurons, especially with HPLC measures of [NAA].

MPTP acts by glial cell conversion to the active neurotoxin, MPP$^+$, which is preferentially taken up by dopaminergic neurons, binds complex I of the mitochondrial electron transport chain of those neurons, and primarily affects the dopaminergic neurons of the SNpc (Jackson-Lewis et al., 1995; Przedborski et al., 2001; Crocker et al., 2003). Because the neurotoxin is reported to have minimal effects on GABAergic neurons (Irwin and Langston, 1985; Javitch et al., 1985; Buck and Amara, 1994; Santiago et

al., 1996; Bezard et al., 1999), we posit that the [NAA] loss in the regions surrounding the SN could reflect glial inflammatory products inducing more widespread changes in neuronal metabolism. Clearly, microglial activation and its subsequent secretory neurotoxic activities have been shown to be an important source of secondary neuronal damage in both the MPTP model and in human PD as well as many other neurodegenerative disorders (McGeer et al., 1988; McGeer and McGeer, 1998; Hunot et al., 1999; Wu et al., 2003) and may affect, in part, mitochondrial function with resulting perturbation of [NAA]. In support of the correlation of migroglial activation and neurodegeneration, postmortem examination of PD patients shows nigrostriatal degeneration associated with significant levels of reactive human leukocyte antigen-DR-positive microglial cells in the SN and is also commonly found in stroke, Alzheimer's disease, and amyotrophic lateral sclerosis (McGeer and McGeer, 1998) Increases in brain cytokine levels are found in the brains and CSF of PD patients (Nagatsu et al., 2000). Microglia produce a plethora of toxic products including proinflammatory cytokines, oxygen-free radicals, quinolinic acid, glutamate, nitric oxide, and others. Oxidative stress and excitotoxicity brought on by activated microglia can by itself lead to nigrostriatal degeneration by activating receptors that contain intracytoplasmic death domains leading to apoptosis (Mochizuki et al., 1996; Anglade et al., 1997; Jenner and Olanow, 1998; Tatton et al., 1998; Olanow and Tatton, 1999). Moreover, in the MPTP model, the degenerative process is perpetuated by a mixture of direct MPP^+-induced damage and microglial toxic activities (Herrera et al., 2000).

Anti-inflammatory drugs such as pioglitazone, a peroxisome proliferator-activated receptor-γ agonist, and the tetracycline derivative minocycline can reduce microglial responses and protect dopaminergic neurons in MPTP animals (Du et al., 2001; He et al., 2001; Breidert et al., 2002; Wu et al., 2002). Vaccination can also attenuate neuronal injury by affecting microglial responses (Moalem et al., 1999; Hammarberg et al., 2000; Hauben et al., 2000; Fisher et al., 2001). This approach may have wide applicability and effectiveness as shown in animal model systems, including neural trauma, glaucoma, ALS, AD, and PD (Krieger et al., 1976; Charness et al., 1989; Janus et al., 2000; Fisher et al., 2001; Hauben et al., 2001, 2003; Lemere et al., 2001; Weiner and Selkoe, 2002; Bakalash et al., 2003).

An unexpected observation made was the degree of [NAA] reduction seen in the SNpc indicated that secondary damage can occur to surrounding glutaminergic and GABAergic neurons (Calon et al., 1999, 2001). TH^+ dopaminergic neurons occupy only 10–30% of total neurons in the ^{1}H MRSI voxel containing the SNpc. However, [NAA] reduction in glutaminergic and GABAergic neurons does not appear causal for neuronal cell death as evidenced by the retention of $Nissl^+$ neuronal counts in all treatment groups. [NAA] loss likely reflects mitochondrial dysfunction that should be reversible.

All together, whether severely affected dopaminergic neurons can be protected from the ravages of PD-associated neurodegeneration using therapeutic strategies outlined in this study is not yet known. However, the data outlined in this report and by others support the idea that such a goal is achievable. Neuroprotective strategies, such as the stereotactic infusion of GDNF, have entered clinical trials and shown benefit as treatments for PD (Gill et al., 2003; Kordower, 2003; Kirik et al., 2004). Having the means available to monitor therapeutic outcomes, such as those described here, will likely prove to be a significant forward step in realizing preventative and regenerative therapeutic goals for PD.

References

Aharoni R, Teitelbaum D, Arnon R, Sela M (1999) Copolymer 1 acts against the immunodominant epitope 82-100 of myelin basic protein by T cell receptor antagonism in addition to major histocompatibility complex blocking. Proc Natl Acad Sci USA 96:634–639.

Angelov DN, Waibel S, Guntinas-Lichius O, Lenzen M, Neiss WF, Tomov TL, Yoles E, Kipnis J, Schori H, Reuter A, Ludolph A, Schwartz M (2003) Therapeutic vaccine for acute and chronic motor neuron diseases: implications for amyotrophic lateral sclerosis. Proc Natl Acad Sci USA 100:4790–4795.

Anglade P, Vyas S, Javoy-Agid F, Herrero MT, Michel PP, Marquez J, Mouatt-Prigent A, Ruberg M, Hirsch EC, Agid Y (1997) Apoptosis and autophagy in nigral neurons of patients with Parkinson's disease. Histol Histopathol 12:25–31.

Baik HM, Choe BY, Son BC, Jeun SS, Kim MC, Lee KS, Kim BS, Lee JM, Lee HK, Suh TS (2003) Proton MR spectroscopic changes in Parkinson's diseases after thalamotomy. Eur J Radiol 47:179–187.

Bakalash S, Kessler A, Mizrahi T, Nussenblatt R, Schwartz M (2003) Antigenic specificity of immunoprotective therapeutic vaccination for glaucoma. Invest Ophthalmol Vis Sci 44:3374–3381.

Benamer HT, Patterson J, Wyper DJ, Hadley DM, Macphee GJ, Grosset DG (2000) Correlation of Parkinson's disease severity and duration with 123I-FP-CIT SPECT striatal uptake. Mov Disord 15:692–698.

Benner EJ, Mosley RL, Destache CJ, Lewis TB, Jackson-Lewis V, Gorantla S, Nemachek C, Green SR, Przedborski S, Gendelman HE (2004) Therapeutic immunization protects dopaminergic neurons in a mouse model of Parkinson's disease. Proc Natl Acad Sci USA 101:9435–9440.

Bernheimer H, Birkmayer W, Hornykiewicz O, Jellinger K, Seitelberger F (1973) Brain dopamine and the syndromes of Parkinson and Huntington. Clinical, morphological and neurochemical correlations. J Neurol Sci 20:415–455.

Bezard E, Gross CE, Fournier MC, Dovero S, Bloch B, Jaber M (1999) Absence of MPTP-induced neuronal death in mice lacking the dopamine transporter. Exp Neurol 155:268–273.

Bezard E, Dovero S, Prunier C, Ravenscroft P, Chalon S, Guilloteau D, Crossman AR, Bioulac B, Brotchie JM, Gross CE (2001) Relationship between the appearance of symptoms and the level of nigrostriatal degeneration in a progressive 1-methyl-4-phenyl-1,2,3,6-tetrahydropyridine-lesioned macaque model of Parkinson's disease. J Neurosci 21:6853–6861.

Boska MD, Nelson JA, Mosley RL, Zelivyanskaya ML, Lewis T, Mellon ML, Gendelman HE (2003) Quantitative mouse brain 1H spectroscopic imaging of an MPTP mouse model of Parkinson's disease using binomial excitation with volume selective refocusing (BEVR). Paper presented at 11th Scientific Meeting and Exhibition of the International Society for Magnetic Resonance in Medicine, Toronto, Ontario, Canada.

Braak H, Braak E (2000) Pathoanatomy of Parkinson's disease. J Neurol 247 [Suppl 2]:II3–II10.

Breidert T, Callebert J, Heneka MT, Landreth G, Launay JM, Hirsch EC (2002) Protective action of the peroxisome proliferator-activated receptor-gamma agonist pioglitazone in a mouse model of Parkinson's disease. J Neurochem 82:615–624.

Brooks DJ (2000) Morphological and functional imaging studies on the diagnosis and progression of Parkinson's disease. J Neurol 247 [Suppl 2]:II11–II18.

Buck KJ, Amara SG (1994) Chimeric dopamine-norepinephrine transporters delineate structural domains influencing selectivity for catecholamines and 1-methyl-4-phenylpyridinium. Proc Natl Acad Sci USA 91:12584–12588.

Burn DJ, O'Brien JT (2003) Use of functional imaging in Parkinsonism and dementia. Mov Disord 18 [Suppl 6]:S88–S95.

Calon F, Morissette M, Goulet M, Grondin R, Blanchet PJ, Bedard PJ, Di Paolo T (1999) Chronic D1 and D2 dopaminomimetic treatment of MPTP-denervated monkeys: effects on basal ganglia GABA(A)/benzodiazepine receptor complex and GABA content. Neurochem Int 35:81–91.

Calon F, Lavertu N, Lemieux AM, Morissette M, Goulet M, Grondin R, Blanchet PJ, Bedard PJ, Di Paolo T (2001) Effect of MPTP-induced denervation on basal ganglia GABA(B) receptors: correlation with dopamine concentrations and dopamine transporter. Synapse 40:225–234.

Ceballos-Baumann AO (2003) Functional imaging in Parkinson's disease: activation studies with PET, fMRI and SPECT. J Neurol 250 [Suppl 1]:I15–I23.

Charness ME, Simon RP, Greenberg DA (1989) Ethanol and the nervous system. N Engl J Med 321:442–454.

Chen JG, Charles HC, Barboriak DP, Doraiswamy PM (2000) Magnetic resonance spectroscopy in Alzheimer's disease: focus on *N*-acetylaspartate. Acta Neurol Scand Suppl 176:20–26.

Chen M, Gran B, Costello K, Johnson K, Martin R, Dhib-Jalbut S (2001) Glatiramer acetate induces a Th2-biased response and crossreactivity with myelin basic protein in patients with MS. Mult Scler 7:209–219.

Chung YL, Barr J, Bhakoo K, Williams SC, Bell JD, Fraser JR (2003) *N*-acetyl aspartate estimation: a potential method for determining neuronal loss in the transmissible spongiform encephalopathies. Neuropathol Appl Neurobiol 29:445–450.

Clark JB (1998) *N*-acetyl aspartate: a marker for neuronal loss or mitochondrial dysfunction. Dev Neurosci 20:271–276.

Clarke CE, Lowry M (2000) Basal ganglia metabolite concentrations in idiopathic Parkinson's disease and multiple system atrophy measured by proton magnetic resonance spectroscopy. Eur J Neurol 7:661–665.

Clarke CE, Lowry M (2001) Systematic review of proton magnetic resonance spectroscopy of the striatum in parkinsonian syndromes. Eur J Neurol 8:573–577.

Clarke CE, Lowry M, Horsman A (1997) Unchanged basal ganglia *N*-acetylaspartate and glutamate in idiopathic Parkinson's disease measured by proton magnetic resonance spectroscopy. Mov Disord 12:297–301.

Crocker SJ, Liston P, Anisman H, Lee CJ, Smith PD, Earl N, Thompson CS, Park DS, Korneluk RG, Robertson GS (2003) Attenuation of MPTP-induced neurotoxicity and behavioural impairment in NSE-XIAP transgenic mice. Neurobiol Dis 12:150–161.

Cruz CJ, Aminoff MJ, Meyerhoff DJ, Graham SH, Weiner MW (1997) Proton MR spectroscopic imaging of the striatum in Parkinson's disease. Magn Reson Imaging 15:619–624.

Dawson TM, Dawson VL (2003) Rare genetic mutations shed light on the pathogenesis of Parkinson disease. J Clin Invest 111:145–151.

DeKosky ST, Marek K (2003) Looking backward to move forward: early detection of neurodegenerative disorders. Science 302:830–834.

Du Y, Ma Z, Lin S, Dodel RC, Gao F, Bales KR, Triarhou LC, Chernet E, Perry KW, Nelson DL, Luecke S, Phebus LA, Bymaster FP, Paul SM (2001) Minocycline prevents nigrostriatal dopaminergic neurodegeneration in the MPTP model of Parkinson's disease. Proc Natl Acad Sci USA 98:14669–14674.

Eidelberg D, Moeller JR, Ishikawa T, Dhawan V, Spetsieris P, Chaly T, Robeson W, Dahl JR, Margouleff D (1995a) Assessment of disease severity in parkinsonism with fluorine-18-fluorodeoxyglucose and PET. J Nucl Med 36:378–383.

Eidelberg D, Moeller JR, Ishikawa T, Dhawan V, Spetsieris P, Chaly T, Belakhlef A, Mandel F, Przedborski S, Fahn S (1995b) Early differential diagnosis of Parkinson's disease with 18F-fluorodeoxyglucose and positron emission tomography. Neurology 45:1995–2004.

Fahn S, Przedborski Sp (2000) Parkinsonism. In: Merritt's neurology, Ed 10 (Rowland LP, ed), pp 679–693. Philadelphia: Lippincott Williams and Wilkins.

Federico F, Simone IL, Lucivero V, Iliceto G, De Mari M, Giannini P, Mezzapesa DM, Tarantino A, Lamberti P (1997) Proton magnetic resonance spectroscopy in Parkinson's disease and atypical parkinsonian disorders. Mov Disord 12:903–909.

Firbank MJ, Harrison RM, O'Brien JT (2002) A comprehensive review of proton magnetic resonance spectroscopy studies in dementia and Parkinson's disease. Dement Geriatr Cogn Disord 14:64–76.

Fisher J, Levkovitch-Verbin H, Schori H, Yoles E, Butovsky O, Kaye JF, Ben-Nun A, Schwartz M (2001) Vaccination for neuroprotection in the mouse optic nerve: implications for optic neuropathies. J Neurosci 21:136–142.

Gao HM, Liu B, Zhang W, Hong JS (2003) Novel anti-inflammatory therapy for Parkinson's disease. Trends Pharmacol Sci 24:395–401.

Garber CE, Friedman JH (2003) Effects of fatigue on physical activity and function in patients with Parkinson's disease. Neurology 60:1119–1124.

Gill SS, Patel NK, Hotton GR, O'Sullivan K, McCarter R, Bunnage M, Brooks DJ, Svendsen CN, Heywood P (2003) Direct brain infusion of glial cell line-derived neurotrophic factor in Parkinson disease. Nat Med 9:589–595.

Gruetter R (1993) Automatic, localized *in vivo* adjustment of all first- and second-order shim coils. Magn Reson Med 29:804–811.

Hammarberg H, Lidman O, Lundberg C, Eltayeb SY, Gielen AW, Muhallab S, Svenningsson A, Linda H, van Der Meide PH, Cullheim S, Olsson T, Piehl F (2000) Neuroprotection by encephalomyelitis: rescue of mechanically injured neurons and neurotrophin production by CNS-infiltrating T and natural killer cells. J Neurosci 20:5283–5291.

Hauben E, Butovsky O, Nevo U, Yoles E, Moalem G, Agranov E, Mor F, Leibowitz-Amit R, Pevsner E, Akselrod S, Neeman M, Cohen IR, Schwartz M (2000) Passive or active immunization with myelin basic protein promotes recovery from spinal cord contusion. J Neurosci 20:6421–6430.

Hauben E, Ibarra A, Mizrahi T, Barouch R, Agranov E, Schwartz M (2001) Vaccination with a Nogo-A-derived peptide after incomplete spinal-cord injury promotes recovery via a T-cell-mediated neuroprotective response: comparison with other myelin antigens. Proc Natl Acad Sci USA 98:15173–15178.

Hauben E, Gothilf A, Cohen A, Butovsky O, Nevo U, Smirnov I, Yoles E, Akselrod S, Schwartz M (2003) Vaccination with dendritic cells pulsed with peptides of myelin basic protein promotes functional recovery from spinal cord injury. J Neurosci 23:8808–8819.

He Y, Appel S, Le W (2001) Minocycline inhibits microglial activation and protects nigral cells after 6-hydroxydopamine injection into mouse striatum. Brain Res 909:187–193.

Herrera AJ, Castano A, Venero JL, Cano J, Machado A (2000) The single intranigral injection of LPS as a new model for studying the selective effects of inflammatory reactions on dopaminergic system. Neurobiol Dis 7:429–447.

Hetherington HP, Pan JW, Mason GF, Ponder SL, Twieg DB, Deutsch G, Mountz J, Pohost GM (1994) 2D 1H spectroscopic imaging of the human brain at 4.1 T. Magn Reson Med 32:530–534.

Hunot S, Dugas N, Faucheux B, Hartmann A, Tardieu M, Debre P, Agid Y, Dugas B, Hirsch EC (1999) FcεRII/CD23 is expressed in Parkinson's disease and induces, *in vitro*, production of nitric oxide and tumor necrosis factor-α in glial cells. J Neurosci 19:3440–3447.

Husted CA, Duijn JH, Matson GB, Maudsley AA, Weiner MW (1994) Molar quantitation of *in vivo* proton metabolites in human brain with 3D magnetic resonance spectroscopic imaging. Magn Reson Imaging 12:661–667.

Irwin I, Langston JW (1985) Selective accumulation of MPP^{+} in the substantia nigra: a key to neurotoxicity? Life Sci 36:207–212.

Jackson-Lewis V, Jakowec M, Burke RE, Przedborski S (1995) Time course and morphology of dopaminergic neuronal death caused by the neurotoxin 1-methyl-4-phenyl-1,2,3,6-tetrahydropyridine. Neurodegeneration 4:257–269.

Janus C, Pearson J, McLaurin J, Mathews PM, Jiang Y, Schmidt SD, Chishti MA, Horne P, Heslin D, French J, Mount HT, Nixon RA, Mercken M, Bergeron C, Fraser PE, St George-Hyslop P, Westaway D (2000) A beta peptide immunization reduces behavioural impairment and plaques in a model of Alzheimer's disease. Nature 408:979–982.

Javitch JA, D'Amato RJ, Strittmatter SM, Snyder SH (1985) Parkinsonism-inducing neurotoxin, *N*-methyl-4-phenyl-1,2,3,6 -tetrahydropyridine: uptake of the metabolite *N*-methyl-4-phenylpyridine by dopamine neurons explains selective toxicity. Proc Natl Acad Sci USA 82:2173–2177.

Jenner P, Olanow CW (1998) Understanding cell death in Parkinson's disease. Ann Neurol 44:S72–S84.

Johnson KP (1996) A review of the clinical efficacy profile of copolymer 1: new U.S. phase III trial data. J Neurol 243:S3–7.

Kipnis J, Schwartz M (2002) Dual action of glatiramer acetate (Cop-1) in the treatment of CNS autoimmune and neurodegenerative disorders. Trends Mol Med 8:319–323.

Kipnis J, Yoles E, Porat Z, Cohen A, Mor F, Sela M, Cohen IR, Schwartz M (2000) T cell immunity to copolymer 1 confers neuroprotection on the damaged optic nerve: possible therapy for optic neuropathies. Proc Natl Acad Sci USA 97:7446–7451.

Kipnis J, Cohen H, Cardon M, Ziv Y, Schwartz M (2004) T cell deficiency leads to cognitive dysfunction: implications for therapeutic vaccination for schizophrenia and other psychiatric conditions. Proc Natl Acad Sci USA 101:8180–8185.

Kirik D, Georgievska B, Bjorklund A (2004) Localized striatal delivery of GDNF as a treatment for Parkinson disease. Nat Neurosci 7:105–110.

Kitada K, Akimitsu T, Shigematsu Y, Kondo A, Maihara T, Yokoi N, Kuramoto T, Sasa M, Serikawa T (2000) Accumulation of *N*-acetyl-L-aspartate in the brain of the tremor rat, a mutant exhibiting absence-like

seizure and spongiform degeneration in the central nervous system. J Neurochem 74:2512–2519.

Kordower JH (2003) *In vivo* gene delivery of glial cell line-derived neurotrophic factor for Parkinson's disease. Ann Neurol 53 [Suppl 3]:S120–S132, S132–S124.

Krieger M, Koeppe Jr RE, Stroud RM (1976) pH dependence of tritium exchange with the C-2 protons of the histidines in bovine trypsin. Biochemistry 15:3458–3464.

Lang AE, Lozano AM (1998) Parkinson's disease. First of two parts. N Engl J Med 339:1044–1053.

Langston JW, Forno LS, Tetrud J, Reeves AG, Kaplan JA, Karluk D (1999) Evidence of active nerve cell degeneration in the substantia nigra of humans years after 1-methyl-4-phenyl-1,2,3,6-tetrahydropyridine exposure. Ann Neurol 46:598–605.

Lemere CA, Maron R, Selkoe DJ, Weiner HL (2001) Nasal vaccination with beta-amyloid peptide for the treatment of Alzheimer's disease. DNA Cell Biol 20:705–711.

Liberatore GT, Jackson-Lewis V, Vukosavic S, Mandir AS, Vila M, McAuliffe WG, Dawson VL, Dawson TM, Przedborski S (1999) Inducible nitric oxide synthase stimulates dopaminergic neurodegeneration in the MPTP model of Parkinson disease. Nat Med 5:1403–1409.

Locascio JJ, Corkin S, Growdon JH (2003) Relation between clinical characteristics of Parkinson's disease and cognitive decline. J Clin Exp Neuropsychol 25:94–109.

Matalon R, Rady PL, Platt KA, Skinner HB, Quast MJ, Campbell GA, Matalon K, Ceci JD, Tyring SK, Nehls M, Surendran S, Wei J, Ezell EL, Szucs S (2000) Knock-out mouse for Canavan disease: a model for gene transfer to the central nervous system. J Gene Med 2:165–175.

McGeer PL, McGeer EG (1998) Mechanisms of cell death in Alzheimer disease–immunopathology. J Neural Transm Suppl 54:159–166.

McGeer PL, Itagaki S, Boyes BE, McGeer EG (1988) Reactive microglia are positive for HLA-DR in the substantia nigra of Parkinson's and Alzheimer's disease brains. Neurology 38:1285–1291.

Moalem G, Leibowitz-Amit R, Yoles E, Mor F, Cohen IR, Schwartz M (1999) Autoimmune T cells protect neurons from secondary degeneration after central nervous system axotomy. Nat Med 5:49–55.

Mochizuki H, Goto K, Mori H, Mizuno Y (1996) Histochemical detection of apoptosis in Parkinson's disease. J Neurol Sci 137:120–123.

Morrish PK, Sawle GV, Brooks DJ (1996) An [18F]dopa-PET and clinical study of the rate of progression in Parkinson's disease. Brain 119:585–591.

Nagatsu T, Mogi M, Ichinose H, Togari A (2000) Cytokines in Parkinson's disease. J Neural Transm Suppl 143–151.

Naressi ACC, Castang I, de Beer R, Graveron-Demilly D (2001) Java-based graphical user interface for MRUI, a software package for quantitation of *in vivo*/medical magnetic resonance spectroscopy signals. Comput Biol Med 31:269.

Ogg RJ, Kingsley PB, Taylor JS (1994) WET, a T1- and B1-insensitive water-suppression method for *in vivo* localized 1H NMR spectroscopy. J Magn Reson B 104:1–10.

Olanow CW, Tatton WG (1999) Etiology and pathogenesis of Parkinson's disease. Annu Rev Neurosci 22:123–144.

Podell M, Maruyama K, Smith M, Hayes KA, Buck WR, Ruehlmann DS, Mathes LE (1999) Frontal lobe neuronal injury correlates to altered function in FIV-infected cats. J Acquir Immune Defic Syndr 22:10–18.

Podell M, Hadjiconstantinou M, Smith MA, Neff NH (2003) Proton magnetic resonance imaging and spectroscopy identify metabolic changes in the striatum in the MPTP feline model of parkinsonism. Exp Neurol 179:159–166.

Przedborski S, Jackson-Lewis V, Naini AB, Jakowec M, Petzinger G, Miller R, Akram M (2001) The parkinsonian toxin 1-methyl-4-phenyl-1,2,3,6-tetrahydropyridine (MPTP): a technical review of its utility and safety. J Neurochem 76:1265–1274.

Sager TN, Laursen H, Hansen AJ (1995) Changes in *N*-acetyl-aspartate content during focal and global brain ischemia of the rat. J Cereb Blood Flow Metab 15:639–646.

Santiago M, Machado A, Cano J (1996) Nigral and striatal comparative study of the neurotoxic action of 1-methyl-4-phenylpyridinium ion: involvement of dopamine uptake system. J Neurochem 66:1182–1190.

Schori H, Kipnis J, Yoles E, WoldeMussie E, Ruiz G, Wheeler LA, Schwartz M (2001) Vaccination for protection of retinal ganglion cells against death from glutamate cytotoxicity and ocular hypertension: implications for glaucoma. Proc Natl Acad Sci USA 98:3398–3403.

Schuff N, Capizzano AA, Du AT, Amend DL, O'Neill J, Norman D, Jagust WJ, Chui HC, Kramer JH, Reed BR, Miller BL, Yaffe K, Weiner MW (2003) Different patterns of *N*-acetylaspartate loss in subcortical ischemic vascular dementia and AD. Neurology 61:358–364.

Seibyl JP, Marek KL, Quinlan D, Sheff K, Zoghbi S, Zea-Ponce Y, Baldwin RM, Fussell B, Smith EO, Charney DS, Hoffer PB, Innis RB (1995) Decreased single-photon emission computed tomographic [123I]beta-CIT striatal uptake correlates with symptom severity in Parkinson's disease. Ann Neurol 38:589–598.

Shults CW (2003) Treatments of Parkinson disease: circa 2003. Arch Neurol 60:1680–1684.

Signoretti S, Marmarou A, Tavazzi B, Lazzarino G, Beaumont A, Vagnozzi R (2001) *N*-acetylaspartate reduction as a measure of injury severity and mitochondrial dysfunction following diffuse traumatic brain injury. J Neurotrauma 18:977–991.

Simpkins N, Jankovic J (2003) Neuroprotection in Parkinson disease. Arch Intern Med 163:1650–1654.

Smallcombe SH, Patt SL, Keifer PA (1995) WET solvent suppression and its applications to LC NMR and high-resolution NMR spectroscopy. J Magn Reson 117:295–303.

Suhy J, Miller RG, Rule R, Schuff N, Licht J, Dronsky V, Gelinas D, Maudsley AA, Weiner MW (2002) Early detection and longitudinal changes in amyotrophic lateral sclerosis by (1)H MRSI. Neurology 58:773–779.

Swindells S, McConnell JR, McComb RD, Gendelman HE (1995) Utility of cerebral proton magnetic resonance spectroscopy in differential diagnosis of HIV-related dementia. J Neurovirol 1:268–274.

Tanji H, Araki T, Nagasawa H, Itoyama Y (1999) Differential vulnerability of dopamine receptors in the mouse brain treated with MPTP. Brain Res 824:224–231.

Tatton NA, Maclean-Fraser A, Tatton WG, Perl DP, Olanow CW (1998) A fluorescent double-labeling method to detect and confirm apoptotic nuclei in Parkinson's disease. Ann Neurol 44:S142–S148.

Tedeschi G, Litvan I, Bonavita S, Bertolino A, Lundbom N, Patronas NJ, Hallett M (1997) Proton magnetic resonance spectroscopic imaging in progressive supranuclear palsy, Parkinson's disease and corticobasal degeneration. Brain 120:1541–1552.

Tedeschi G, Bonavita S, McFarland HF, Richert N, Duyn JH, Frank JA (2002) Proton MR spectroscopic imaging in multiple sclerosis. Neuroradiology 44:37–42.

Teitelbaum D, Arnon R, Sela M (1997) Cop 1 as a candidate drug for multiple sclerosis. J Neural Transm Suppl 49:85–91.

Vanhamme L, van den Boogaart A, Van Huffel S (1997) Improved method for accurate and efficient quantification of MRS data with use of prior knowledge. J Magn Reson 129:35–43.

Vielhaber S, Kudin AP, Kudina TA, Stiller D, Scheich H, Schoenfeld A, Feistner H, Heinze HJ, Elger CE, Kunz WS (2003) Hippocampal *N*-acetyl aspartate levels do not mirror neuronal cell densities in creatine-supplemented epileptic rats. Eur J Neurosci 18:2292–2300.

Vingerhoets FJ, Snow BJ, Lee CS, Schulzer M, Mak E, Calne DB (1994) Longitudinal fluorodopa positron emission tomographic studies of the evolution of idiopathic parkinsonism. Ann Neurol 36:759–764.

Weiner HL, Selkoe DJ (2002) Inflammation and therapeutic vaccination in CNS diseases. Nature 420:879–884.

Wolters EC (2000) Psychiatric complications in Parkinson's disease. J Neural Transm Suppl 291–302.

Wolters EC (2001) Psychiatric complications in the treatment of Parkinson's disease. Adv Neurol 86:385–393.

Woods RP, Grafton ST, Holmes CJ, Cherry SR, Mazziotta JC (1998) Automated image registration: I. General methods and intrasubject, intramodality validation. J Comput Assist Tomogr 22:139–152.

Wu DC, Jackson-Lewis V, Vila M, Tieu K, Teismann P, Vadseth C, Choi DK, Ischiropoulos H, Przedborski S (2002) Blockade of microglial activation is neuroprotective in the 1-methyl-4-phenyl-1,2,3,6-tetrahydropyridine mouse model of Parkinson disease. J Neurosci 22:1763–1771.

Wu DC, Teismann P, Tieu K, Vila M, Jackson-Lewis V, Ischiropoulos H, Przedborski S (2003) NADPH oxidase mediates oxidative stress in the 1-methyl-4-phenyl-1,2,3,6-tetrahydropyridine model of Parkinson's disease. Proc Natl Acad Sci USA 100:6145–6150.